The Company of **Biologists**

SHORT REPORT

Citron kinase-dependent F-actin maintenance at midbody secondary ingression sites mediates abscission

Alessandro Dema[1,2], Francesca Macaluso[1], Francesco Sgrò[1], Gaia E. Berto[1,3], Federico T. Bianchi[1,3], Alessandra A. Chiotto[1,3], Gianmarco Pallavicini[1,3], Ferdinando Di Cunto[1,3,4,*] and Marta Gai[1,*]

ABSTRACT

Abscission is the final step of cytokinesis whereby the intercellular bridge (ICB) linking the two daughter cells is cut. The ICB contains a structure called the midbody, required for the recruitment and organization of the abscission machinery. Final midbody severing is mediated by formation of secondary midbody ingression sites, where the ESCRT III component CHMP4B is recruited to mediate membrane fusion. It is presently unknown how cytoskeletal elements cooperate with CHMP4B to mediate abscission. Here, we show that F-actin is associated with midbody secondary sites and is necessary for abscission. F-actin localization at secondary sites depends on the activity of RhoA and on the abscission regulator citron kinase (CITK). CITK depletion accelerates loss of F-actin proteins at the midbody and subsequent cytokinesis defects are reversed by restoring actin polymerization. Conversely, midbody hyperstabilization produced by overexpression of CITK and ANLN is reversed by actin depolymerization. CITK is required for localization of F-actin and ANLN at the abscission sites, as well as for CHMP4B recruitment. These results indicate that control of actin dynamics downstream of CITK prepares the abscission site for the final cut.

KEY WORDS: ESCRT-III, Abscission, Actin, Citron kinase, Cytokinesis, Midbody

INTRODUCTION

Cytokinesis is the terminal step of cell division that leads to the physical separation of daughter cells. The actomyosin contractile machinery drives ingression of the cleavage furrow (Eggert et al., 2006; Pollard, 2010). Actomyosin ring assembly and contraction are promoted by the small GTPase RhoA and its stabilization is regulated by ANLN, one of the crucial RhoA partners during cytokinesis (Piekny and Glotzer, 2008). Furrow constriction allows the formation of an intercellular bridge (ICB) containing bundles of antiparallel microtubules, which overlap at the midbody (Mierzwa and Gerlich, 2014). This structure provides a platform for the recruitment and organization of many proteins that regulate abscission (Agromayor and Martin-Serrano, 2013; Mierzwa and Gerlich, 2014).

[1]Dept. of Molecular Biotechnology and Health Sciences, University of Turin, 10126 Turin, Italy. [2]FMP-Berlin Campus Berlin-Buch, Robert-Roessle-Str. 10, 13125 Berlin, Germany. [3]Neuroscience Institute Cavalieri Ottolenghi, Turin, 10043 Orbassano Italy. [4]Neuroscience Institute of Turin (NIT), 10043 Orbassano, Italy.

*Authors for correspondence (marta.gai@unito.it; ferdinando.dicunto@unito.it)

A.D., 0000-0003-0976-9396; F.S., 0000-0002-2062-4908; G.E.B., 0000-0001-5963-6298; A.A.C., 0000-0002-9692-1714; F.D., 0000-0001-9367-6357; M.G., 0000-0002-9819-1743
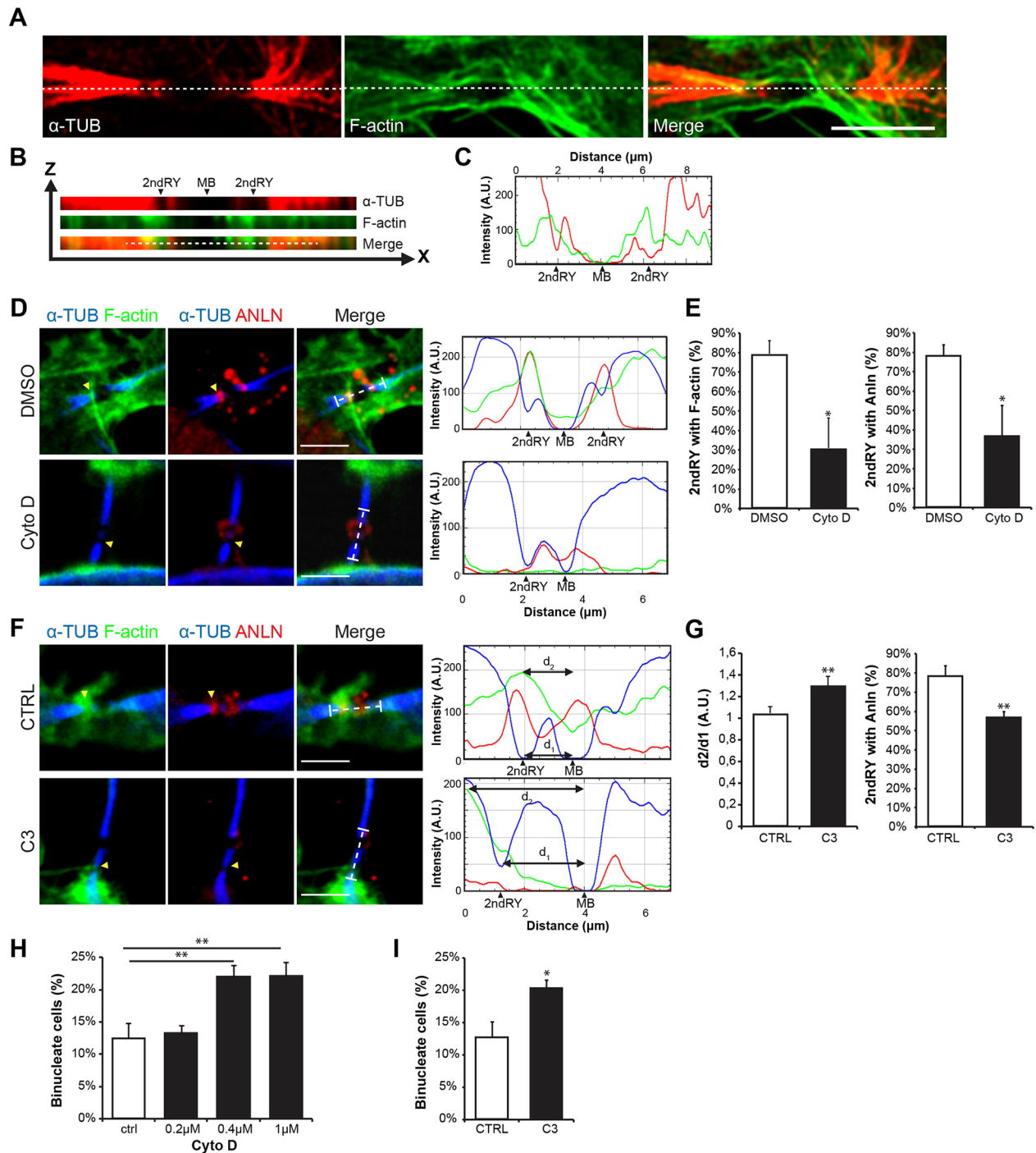
After cleavage furrow ingression, the midbody is mechanically stabilized and anchored to the cell cortex by multiple mechanisms (Mierzwa and Gerlich, 2014). The ICB gradually narrows (Guizetti et al., 2011; Schiel et al., 2012) and two constriction zones, also called secondary ingression sites, form at both sides of the midbody (Elia et al., 2011; Guizetti et al., 2011; Schiel et al., 2011, 2012). The ESCRT-III complex consists of numerous charged multivesicular body proteins (CHMPs) and is required to execute abscission. First, it is recruited at the midbody, then it is relocalized to constriction sites marking where the abscission occurs (Elia et al., 2011; Guizetti et al., 2011).

It is poorly understood how late midbody structures are organized. None of the microtubule-interacting proteins so far involved in cytokinesis has been found to localize in secondary ingression sites, whereas cleavage furrow proteins, such as ANLN and RhoA, localize not only to the furrow cortex and midbody, but also to constriction zones (Hu et al., 2012). It has been proposed that the ANLN-septin cytoskeleton primes the ICB for recruitment of the ESCRT-III subunit CHMP4B, leading to abscission (Renshaw et al., 2014). The localization of RhoA and ANLN at the midbody during late stages of cytokinesis depends on CITK, a protein required for spindle positioning (Gai et al., 2011) and abscission (Bassi et al., 2011, 2013; El Amine et al., 2013; Gai et al., 2011; McKenzie et al., 2016; Watanabe et al., 2013). It has been demonstrated that CITK stabilizes midbody architecture by binding components of the contractile ring (ANLN, myosin and RhoA), central spindle (KIF23/MKLP1, KIF14) and the chromosomal passenger complex (Bassi et al., 2011, 2013; Gai et al., 2011; Gruneberg et al., 2006; McKenzie et al., 2016; Watanabe et al., 2013). Moreover, CITK stabilizes midbody microtubules by increasing the phosphorylation of TUBB3 (Sgrò et al., 2015).

These data suggest that CITK, together with ANLN and RhoA, could have a late role in cytokinesis, mediating ICB constriction and the final cut. In this report, we investigated whether the regulation of actin dynamics could control abscission by affecting formation and maturation of the constriction zone, and addressed the possible role of CITK and its partner ANLN in this stage of cytokinesis.

RESULTS AND DISCUSSION
F-actin is required for normal abscission

To start assessing the role of F-actin in abscission, we analyzed its organization in late midbodies, using super-resolution microscopy (Fig. 1A). Interestingly, we found that a small pool of F-actin colocalizes at secondary ingression sites (Fig. 1A-C) with ANLN (Fig. 1D,F). To address whether F-actin localization at secondary sites is necessary for ANLN localization, we treated synchronized HeLa cells with Cytochalasin D (CytoD). To avoid the detrimental effects of actin depolymerization on early cytokinesis stages, treatment was performed after complete cleavage furrow ingression

Fig. 1. F-actin localizes at secondary ingression sites and is required for abscission. (A) Intercellular bridge (ICB) of HeLa cells stained for α-tubulin and F-actin. Images were acquired using super-resolution confocal microscopy. Dotted lines indicate the plane of cross section (x-z) shown in B. (C) Intensity profile, plotted for the two channels along the ICB (dotted line). (D-G) HeLa cells synchronized in late cytokinesis, treated for 60 min with 0.4 μM CytoD or DMSO (D,E) and with C3 transferase or control solution (F,G) and immunostained for α-tubulin, ANLN and F-actin. Images were acquired using confocal microscopy. Yellow arrowheads indicate secondary ingression sites. Intensity profile is plotted on the right for the three channels along the ICB (dotted line). (E) Quantification of the percentage of secondary ingression sites positive for F-actin and ANLN, in midbodies of cells treated as in D (n>50, N=3). (G) Quantification of F-actin distribution (left histogram) and of the percentage of secondary ingression sites positive for ANLN, in midbodies of cells treated as in F (n>50, N=3).
(H,I) Cells synchronized as in D-G, treated either with increasing concentration of CytoD (H) or with C3 transferase (I) and fixed 180 min after addition of the drug. The percentage of binucleated cells was determined by DAPI and α-tubulin staining and fluorescence microscopy (n>300 cells, N=3). Scale bars: 5 μm. MB, midbody; 2ndRY, secondary ingression sites. Data shown in histograms are means±s.e.m. Statistical significance was assessed using a two-tailed Student's t-test. **$P<0.01$; *$P<0.05$.

at 120 min after release from nocodazole. This treatment decreased F-actin localization at the midbody, but did not significantly alter the intensity of cell body fluorescence (Fig. S1A). The actual number of secondary sites was not significantly different (Fig. S1B), but F-actin and ANLN were lost from these structures (Fig. 1D,E).
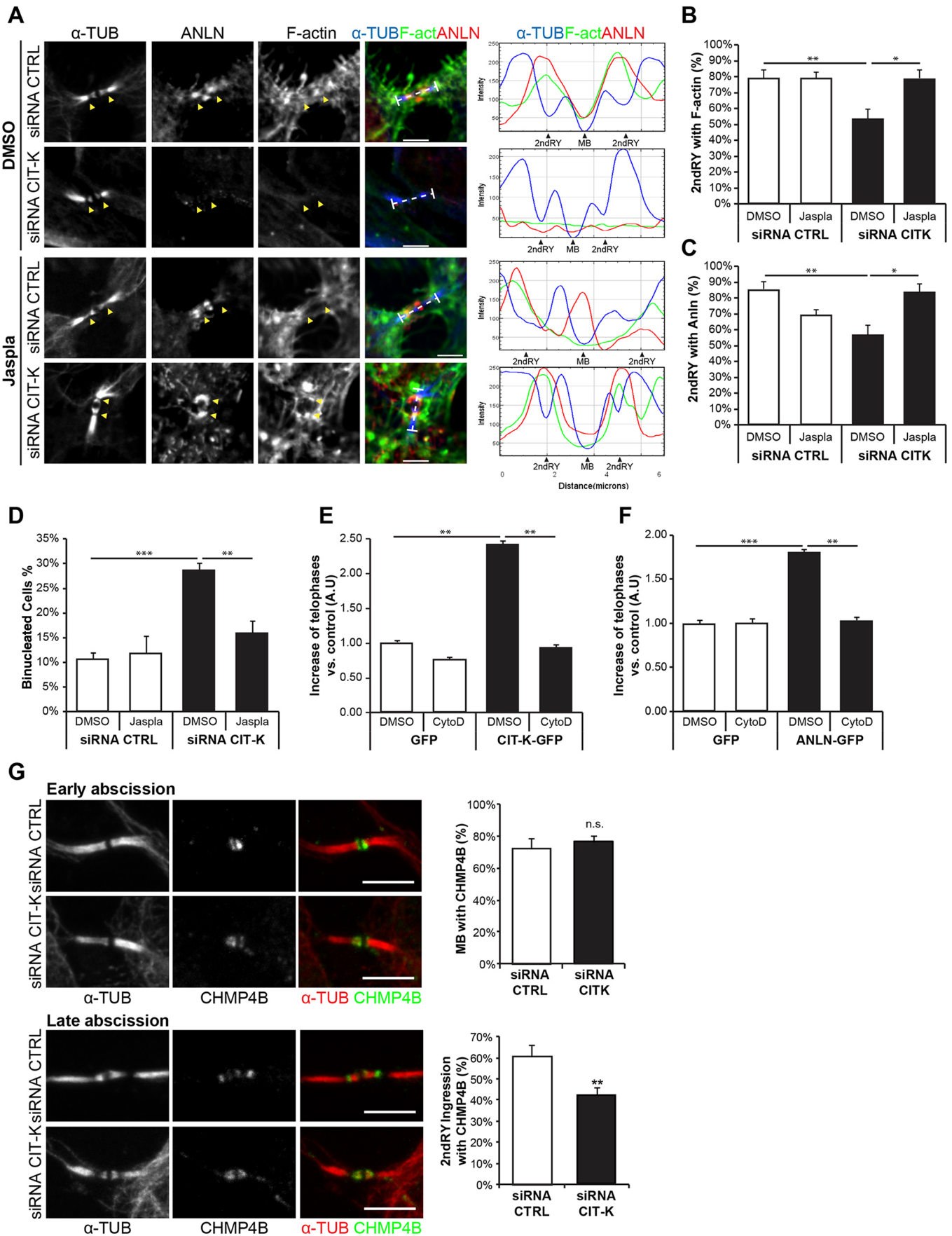
Fig. 2. See next page for legend.

Fig. 2. CITK is required for localization of F-actin, ANLN and CHMP4B at secondary ingression sites. (A) HeLa cells treated with control or CITK siRNAs were synchronized in late cytokinesis, treated with 10 nM Jasplakinolide or DMSO for 60 min and immunostained for α-tubulin, ANLN and F-actin. Images were acquired using confocal microscopy. Yellow arrowheads indicate secondary ingression sites. Intensity profiles are plotted on the right for the three channels along the ICB (dotted line). (B,C) Quantification of the percentage of secondary ingression sites positive for F-actin (B) and ANLN (C) in midbodies of cells treated as in A ($n>50$, $N=3$). (D) HeLa cells, transfected with control or CITK siRNAs, were treated as in A and fixed after 180 min following Jasplakinolide addition. The percentage of binucleated cells was determined by DAPI and α-tubulin staining followed by fluorescence microscopy ($n>300$ cells, $N=3$). (E,F) HeLa cells transfected with GFP, CITK-GFP or ANLN-GFP, synchronized as in A and treated with 1 μM CytoD or DMSO, fixed after 60 min and stained with DAPI and α-tubulin. Abscission delay was evaluated by measuring the relative increase of telophases in cells overexpressing CITK and ANLN, versus control cells ($n>300$, $N=5$). (G) HeLa cells treated as in A immunostained for α-tubulin and CHMP4B. Images were acquired using confocal microscopy. Cells in telophase were considered to be early or late abscissions based on the presence of secondary ingression sites. Percentage of either midbodies (top) or secondary ingression sites (bottom) positive for CHMP4B was quantified. ($n>50$, $N=4$). Scale bars: 5 μm. MB, midbody; 2ndRY, secondary ingression sites. Data shown in histograms are means±s.e.m. Statistical significance was assessed using a two-tailed Student's *t*-test. ***$P<0.001$; **$P<0.01$; *$P<0.05$; n.s., not significant.

Next, to assess the role of RhoA on localization of F-actin and ANLN in the late midbody, we treated HeLa cells with the Rho inhibitor C3 transferase, upon complete furrow ingression. After this treatment, F-actin intensity decreased more in the midbody than in the cell body (Fig. S1C) and was not correctly distributed along the ICB: its accumulation was not centered on the secondary ingression sites (Fig. 1F,G). Even in this case, ANLN failed to localize at constriction sites (Fig. 1F,G).

Treatment of late cytokinesis cells with CytoD concentrations of 0.4 μM or higher induced a significant increase in the number of binucleated cells (Fig. 1H). A similar effect was induced by RhoA inhibition by treatment with C3 transferase (Fig. 1I). To confirm that binucleation was due to cytokinesis failure after midbody formation, we observed control and treated cells in telophase at the time of drug addition using time-lapse microscopy (Fig. S1D, Movies 1 and 2). The number of cells that failed cytokinesis after cleavage ingression was significantly increased by CytoD treatment (Fig. S1E). Together, these results indicate that ANLN localization at secondary sites depends on the presence of F-actin at the midbody and that correct localization of both F-actin and ANLN depends on RhoA activity. Moreover, these observations suggest that localized RhoA activity is required to maintain a small pool of F-actin and to recruit ANLN at the secondary ingression sites. Most importantly, they demonstrate that these events are functionally relevant for correct abscission.

CITK controls localization of F-actin, ANLN and CHMP4B in secondary ingression sites

CITK is required to maintain ANLN and active RhoA at the midbody in late cytokinesis (Gai et al., 2011). We therefore asked whether this protein is also necessary for proper cytoskeletal organization at secondary ingression sites. Quantitative analysis of late midbodies showed that both F-actin and ANLN are decreased at secondary sites in CITK-depleted cells, as compared to levels in the control (Fig. 2A-C), whereas their overall abundance in cytoplasm is not significantly different (data not shown). Altered F-actin and ANLN localization is likely to be produced by increased F-actin depolymerization. Indeed, treatment of cells with the actin stabilizer

Jasplakinolide restored the localization of both F-actin and ANLN (Fig. 2A-C). To assess if control of actin stability is an event downstream of CITK that is important for abscission, we studied whether actin stabilization can prevent the cytokinesis failure induced by CITK loss. To this aim, we allowed control and CITK-depleted cells treated with Jasplakinolide to exit mitosis and quantified the percentage of binucleated cells. Interestingly, Jasplakinolide did not modify binucleation frequency in cells treated with control siRNA, but it reverted to control levels the increased binucleation frequency produced by CITK loss (Fig. 2D).

We previously showed that CITK overexpression leads to midbody hyper-stabilization through RhoA activation, doubling abscission time (Gai et al., 2011). ANLN overexpression induces the same phenotype, acting downstream of RhoA (Gai et al., 2011). Consequently, the percentage of cells in cytokinesis 180 min after nocodazole release was significantly increased by CITK or ANLN overexpression (Gai et al., 2011; Fig. 2E,F). To assess the role of actin dynamics in these phenotypes, we treated telophase-synchronized HeLa cells overexpressing CITK or ANLN with CytoD. Actin depolymerization restored cytokinesis progression to levels of the corresponding controls in both cases (Fig. 2E,F), and reverted the increased levels of midbody F-actin produced by CITK overexpression (Fig. S2A). RhoA inhibition through C3 transferase reverts the abscission delay caused by CITK overexpression (Gai et al., 2011). Accordingly, F-actin levels at the midbody of CITK-overexpressing cells were restored to normal values by RhoA inhibition (Fig. S2B), confirming that CITK downstream events in late midbodies depend on RhoA activity (Gai et al., 2011).

Altogether, these results indicate that CITK regulates F-actin levels at the midbody in late cytokinesis, and support a critical role of actin stability in the CITK-RhoA-actin-ANLN pathway, leading to abscission. Since the ANLN-septin complex primes the ICB for CHMP4B recruitment at the abscission site (Renshaw et al., 2014), we analyzed whether CHMP4B is disturbed by CITK depletion. In CITK-depleted cells, CHMP4B was correctly associated with the midbody (Fig. 2G), but it did not localize to secondary sites (Fig. 2G). This suggests that CITK is required for CHMP4B relocalization from the midbody to constriction sites.

CITK and ANLN influence actin dynamics at the midbody

To directly assess whether CITK controls actin dynamics in late cytokinesis, we transfected cells with the live-imaging tracer Lifeact-RFP, which specifically associates with actin filaments (Riedl et al., 2008), and measured its fluorescence intensity at midbody at fixed times after this structure was formed. In control cells, the Lifeact-RFP signal accumulated at the cleavage furrow during its constriction (Fig. 3A, Movie 3). F-actin accumulation remained readily detectable after midbody formation, but it progressively decreased during midbody maturation (Fig. 3B). Nevertheless, in half of cell divisions, after the Lifeact-RFP signal reached 20% of the initial intensity, we could detect a late spike in fluorescence just before abscission (Fig. 3B,C,G).

When CITK was depleted, actin disassembly was faster than in control cells (Fig. 3E, Movies 3 and 4). Indeed, the time required for the reduction of Lifeact-RFP midbody signal from 100% to 20% was significantly decreased (Fig. 3F). Moreover, the frequency of Lifeact spikes was decreased to approximately half that of the control (Fig. 3G).

To check if the effect of CITK on actin dynamics is global or local, we biochemically assessed whether CITK depletion alters the ratio between monomeric (G) and filamentous (F) actin, by
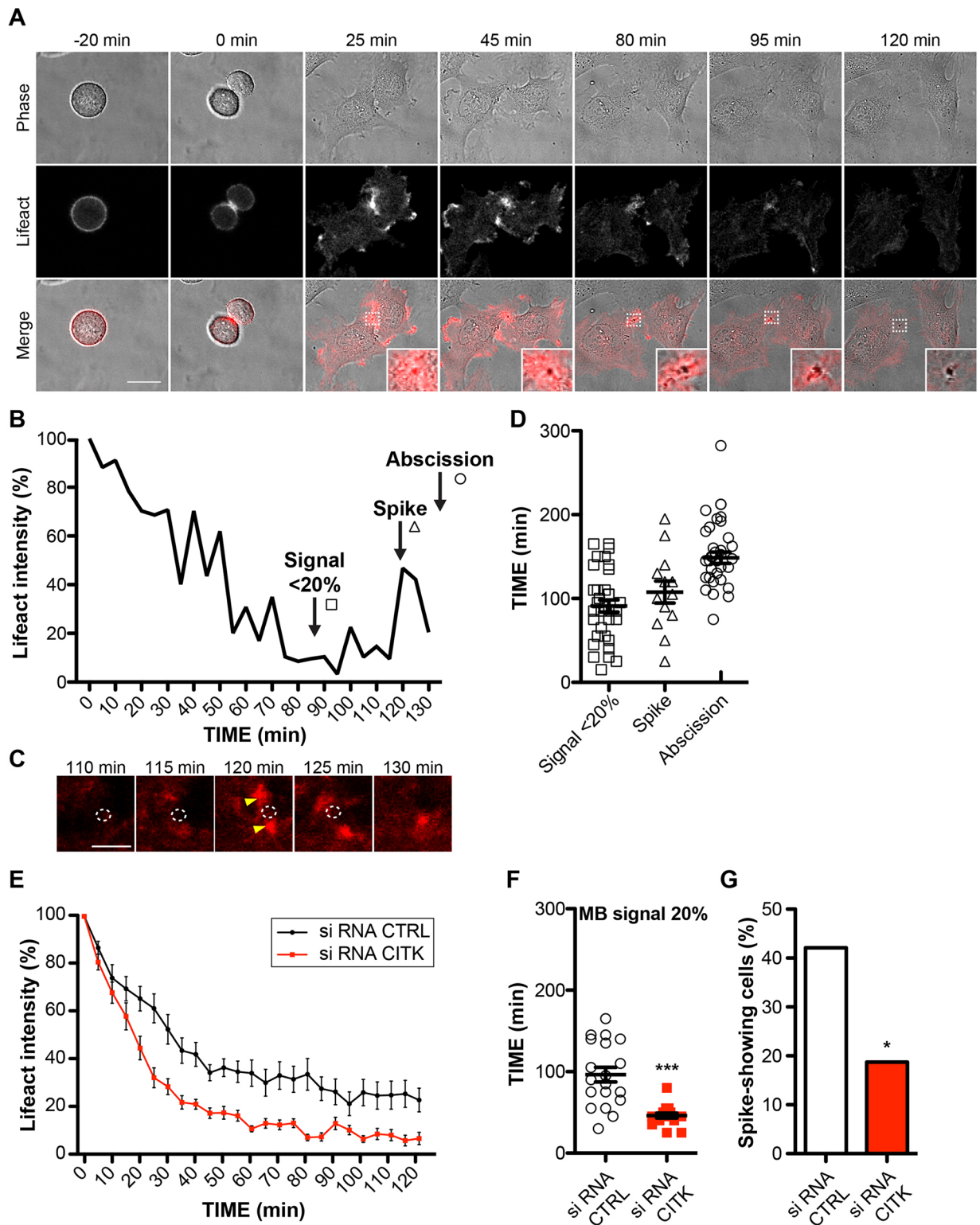
Fig. 3. CITK depletion speeds up F-actin disassembly from the midbody. (A) Selected frames from time-lapse imaging experiments of HeLa cells undergoing cytokinesis (Movies 3 and 4). HeLa cells were transfected with Lifeact-RFP and observed 30 h post-transfection. Scale bars: 20 µm. (B-G) Fluorescence intensity of Lifeact-RFP at the midbody was analyzed in control and CITK-depleted HeLa cells every 5 min for 120 min after cleavage furrow ingression (time 0). Lifeact-RFP intensity at time 0 was set as 100%. (B) Example of intensity profile of midbody Lifeact-RFP from completion of cleavage furrow ingression to abscission. F-actin disassembly (MB signal <20%), second spike of actin polymerization and abscission are indicated. (C) Zoomed images from time-lapse experiment showing a spike (yellow arrowheads) in actin polymerization at the midbody (white circle). (D) Distribution and average of times required in control cells for F-actin disassembly (MB signal <20%), second spike of actin polymerization and abscission. (E) Normalized values of Lifeact intensity at the midbody in control and CITK-depleted HeLa cells. (F) Time for F-actin disassembly in control and CITK-depleted HeLa cells. Data shown in histograms are means±s.e.m. Statistical significance was assessed using a two-tailed Student's *t*-test. ***$P<0.001$; $n>10$ cells. (G) Percentage of cytokinesis with the second spike of actin polymerization. Statistical significance was assessed using a Chi-square test. *$P<0.05$ ($n>10$, $N=3$). Scale bars: 10 µm.
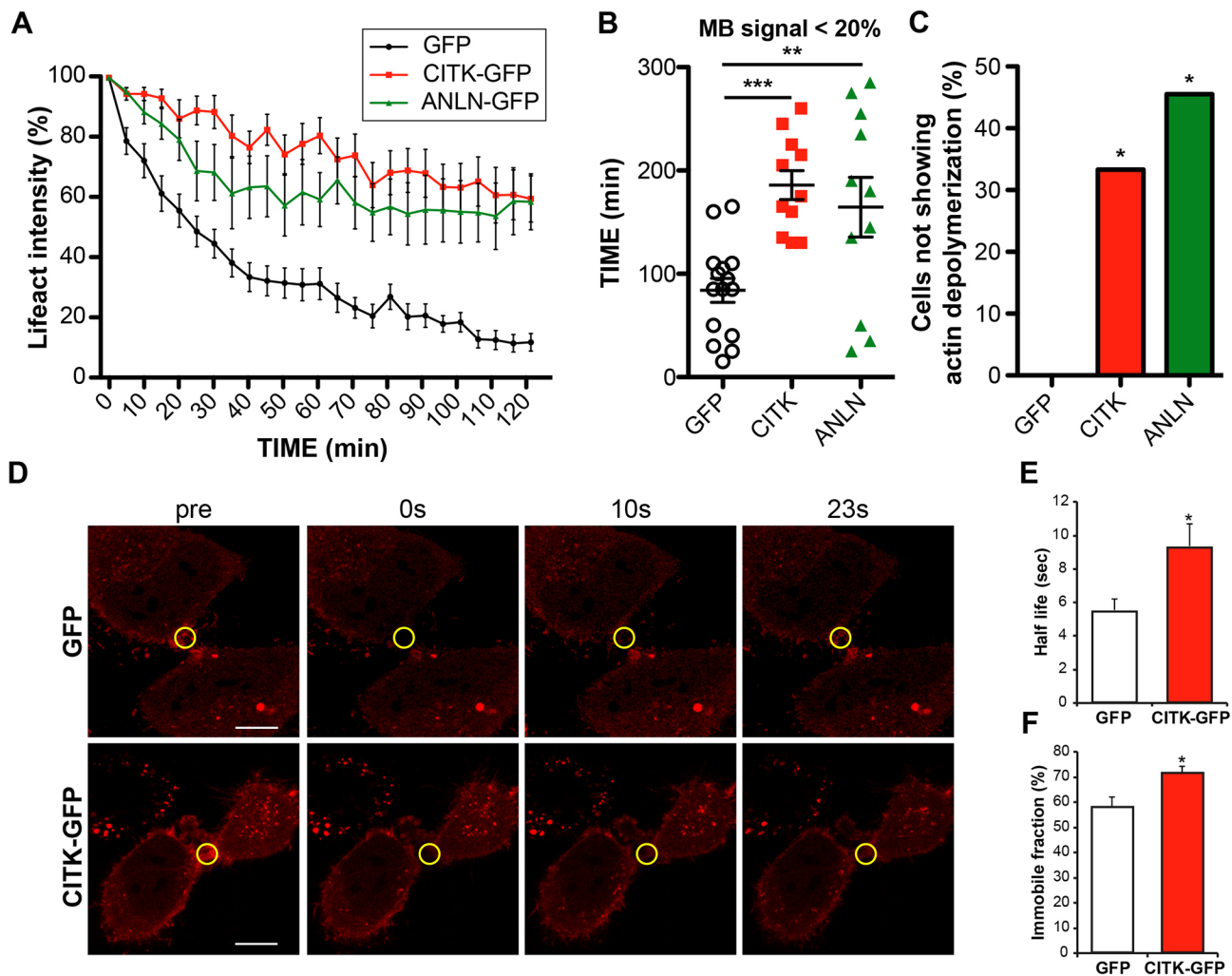
Fig. 4. CITK and ANLN overexpression stabilizes F-actin in the midbody. HeLa cells transfected with Lifeact-RFP observed 30 h post-transfection. (A) Fluorescence intensity of Lifeact-RFP at the midbody analyzed in HeLa cells expressing either GFP, CITK-GFP or ANLN-GFP (Movies 5-7). Time 0 was set when cleavage furrow ingression was completed; Lifeact-RFP intensity of time 0 was set to 100%. (B) Time for F-actin intensity decrease from 100 to 20% (MB signal <20%) calculated in cells treated as in A. Statistical significance was assessed using a two-tailed Student's *t*-test. ***P<0.001; **P<0.01. (C) Quantification of the percentage of cytokinesis without actin depolymerization from the midbody in cells treated as in A. Statistical significance was assessed using a Chi-square test. *P<0.05 (*n*>10, *N*=3). (D-F) Actin dynamics were analyzed by FRAP analysis in HeLa cells transfected with RFP-actin with either CITK-GFP or GFP. (D) Selected frames of FRAP experiments before (pre) and after bleaching, and throughout the recovery. Yellow circle indicates the ROI used for FRAP analysis. Scale bars: 10 μm. (E,F) Half-life and immobile fraction of actin in the midbody (*n*>10, *N*=3). Data shown in histograms are means±s.e.m. Statistical significance was assessed using a two-tailed Student's *t*-test. *P<0.05.

detergent-based cell fractionation. We could not detect any difference in G-actin/F-actin (G/F) ratio in control versus CITK-depleted cells (Fig. S3A,B). This result supports the hypothesis that the effect of CITK on F-actin is temporally and spatially regulated.

When HeLa cells were transfected with a plasmid overexpressing GFP-tagged CITK or ANLN protein, we observed a reduction in the rate of decrease of midbody actin (Fig. 4A, Movies 5-7). Indeed, in CITK- and ANLN-overexpressing cells, the time required for Lifeact-RFP midbody signal to reduce to 20% was significantly longer than it was in the control (Fig. 4B). Moreover, there was an increase of divisions in which the Lifeact-RFP fluorescence intensity at the midbody never dropped below 20% of the starting value (Fig. 4C). We observed a decrease of the G/F ratio in CITK-transfected cultures (Fig. S3C,D), suggesting that its overexpression exerts a dominant effect on actin polymerization. To directly evaluate whether CITK affects F-actin dynamics at the midbody, we used fluorescence recovery after photobleaching (FRAP) of RFP-

actin, performed at the midbodies of cells overexpressing CITK or control plasmid (Fig. 4D). CITK increased both RFP-actin recovery half-life and the immobile fraction (Fig. 4E,F). These results indicate that CITK controls the disassembly of F-actin at the midbody during late cytokinesis, possibly decreasing the F-actin turnover rate, and suggest that ANLN may be relevant for this function.

Conclusion

In this report, we provide evidence that F-actin assembly and disassembly from the ICB in the late cytokinesis stages is finely regulated. Upon complete cleavage furrow ingression, most actin filaments of the actomyosin ring disassemble (Dambournet et al., 2011; Guizetti et al., 2011; Saurin et al., 2008; Schiel et al., 2012). However, a small pool of F-actin is maintained at secondary ingression sites, where F-actin colocalizes with ANLN. Moreover, we showed that maintenance of F-actin at secondary sites may be functionally

relevant for abscission and that CITK has a fundamental role in this process. When CITK is missing, polymerized actin is prematurely removed and ANLN is not stabilized at the midbody. These events may end up with lack of CHMP4B relocalization at abscission sites and cytokinesis failure. Conversely, when CITK is overexpressed, F-actin disassembly from the midbody is slowed down and abscission is delayed, consistent with previous findings (Gai et al., 2011). Therefore, CITK is required not only for midbody stabilization, as previously demonstrated (Bassi et al., 2013; Gai et al., 2011; Mckenzie et al., 2016), but also for midbody late-stage maturation and the final cut. Since CITK does not itself localize to secondary sites (Hu et al., 2012), it is possible that its catalytic activity may drive post-translational modifications on ANLN and/or on other players that need to be localized there. Further studies will be necessary to investigate these possibilities.

MATERIALS AND METHODS
Cell culture, synchronization and drug treatments
Unmodified HeLa cells were originally obtained from ATCC and a new batch was thawed after 5 passages. All cells are routinely screened for mycoplasma contamination. HeLa cells were cultured in RPMI medium supplemented with 10% fetal bovine serum (FBS) and 1% penicillin/streptomycin. The HeLa cell line expressing α-tubulin–GFP was maintained in DMEM-GlutaMAX (Invitrogen) supplemented with 10% FBS, 100 U ml^{-1} penicillin, 100 µg ml^{-1} streptomycin, 200 µg ml^{-1} Geneticin (Sigma, St Louis, MO, USA) and 0.5 µg ml^{-1} puromycin. All cells were cultured in a humidified 5% CO$_2$ incubator at 37°C.

For synchronization, asynchronous cultures were supplemented with 25 µg/ml Aphidicolin (Sigma) and maintained under these conditions for 24 h and then cultured for a further 16 h in fresh complete medium in the presence of 50 ng/ml nocodazole (Sigma) to block cells at prometaphase. Finally, cells were washed three times with fresh medium and allowed to progress through mitosis/cytokinesis for the indicated times.

For time-lapse imaging, HeLa cells were synchronized by a double-thymidine block: asynchronous cultures were treated with 2 mM thymidine (Sigma) for 16 h, then released for 4-6 h in fresh complete medium and again blocked for 16 h. Finally, cells were washed twice with fresh medium and allowed to progress through mitosis.

For drug treatments, synchronized HeLa cells were treated with 0.2, 0.4 and 1 µM Cytochalasin D (Sigma), 10 nM Jasplakinolide (Merck) and Rho inhibitor C3 transferase as described.

Plasmids, siRNAs and cell transfection
In this study, we used a previously validated CITK-siRNA sequence (AUGGAAGGCACUAUUUCUCAA) (Gai et al., 2011) obtained from GE-Healthcare (Dharmacon, Lafayette, CO). The ON-TARGETplus non-targeting siRNA #1 (GE Healthcare, Dharmacon) was used as a negative control for potential off-target effects. The expression construct coding for CITK-GFP was generated by inserting the Myc-CITK cDNA into the pm-GFP-N1 plasmid (Clontech, Mountain View, CA) (Gai et al., 2011). The GFP-ANLN construct was kindly provided by Alisa Piekny (Piekny and Glotzer, 2008). Transfection was performed with Lipofectamine 2000 (Invitrogen) for siRNA and with TransIT-Lt1 (Mirus) for plasmids, following standard manufacturer's protocols.

Antibodies
The following antibodies were used: mouse anti-α-tubulin, 1:1000 (Sigma, T5168, clone B-5-1-2); rabbit polyclonal anti-ANLN, 1:200 (Bethyl laboratories, a301-406a); rabbit anti-CHMP4B, 1:1000 (provided by Harald Stenmark, The Norwegian Radium Hospital, Oslo, Norway), rabbit polyclonal anti-actin (Santa Cruz, sc-7210); rabbit anti-GFP, western blot 1:2000 (Abcam, ab290).

Immunofluorescence
Cells were fixed in 4% paraformaldehyde at room temperature for 10 min for ANLN and actin staining or with methanol at −20°C for 10 min for CHMP4B staining. In all cases, cells were permeabilized in 0.1% Triton X-100 in PBS

for 10 min, saturated in 5% BSA in PBS for 30 min and incubated with primary antibody for 45 min at room temperature. Primary antibodies were detected with anti-rabbit or anti-mouse Alexa Fluor 488/568/647 (Molecular Probes, Invitrogen), used at 1:1000 dilution for 30 min. For F-actin staining, Acti-stain 488 Phalloidin (Cytoskeleton Denver, CO) was used in accordance with the manufacturer's instructions. Counterstaining was performed with the DNA dye DAPI (Sigma) at 0.5 µg/ml for 1 min.

Western blotting and G-actin/F-actin quantification
Western blotting was performed following standard protocols. For G/F quantification, unsynchronized HeLa cells were firstly lysed in a solution containing 30% glycerol and 1% Triton X-100, buffered with PIPES, EGTA and MgSO$_4$, and the lysate was considered to represent the cytosolic fraction. The resulting pellets were then lysed again in a solution containing 1.5% SDS and 25 mM Tris-HCl, pH 6.8 at 95°C; the resulting lysate contained the cytoskeletal elements.

Microscopy
Imaging was performed using a Leica TCS SP5 confocal system (Leica Microsystems) equipped with a 405 nm diode, an argon ion, a 561 nm DPSS and a HeNe 633 nm lasers. Fixed cells were imaged using a HCX PL APO 63×/1.4 NA oil immersion objective. For live imaging, time lapses were recorded overnight with an interval of 5 min using a 40× PlanApo N.A. 1.4 oil immersion objective on the cells kept in the microscope incubator at 37°C and 5% CO$_2$.

FRAP experiments were performed on midbodies of constant size using 100% transmission of 568 nm laser for photobleaching. Recovery kinetics were then measured and, after background subtraction, were normalized to pre-bleach frames. Super-resolution images were obtained using a Leica SP8 confocal system with HyVolution 2 (Leica Microsystems) equipped with an argon ion, a 561 nm DPSS and a HeNe 633 nm lasers. Fixed cells were imaged using a HCX PL APO 63×/1.4 NA oil immersion objective. Series of x-y-z images (typically 0.04×0.04×0.106 µm^3 voxel size) were collected.

Image analysis
HeLa cells expressing Lifeact-RFP were imaged from anaphase to abscission using a Leica SP5 confocal laser-scanning microscope, with red fluorescence and DIC frames acquired every 5 min. We acquired images with low laser power and frame rate in order to avoid bleaching. The intensity of Lifeact fluorescence at the midbody was evaluated with ImageJ in an area of fixed surface manually imposed on the midbody ring, identified by the DIC image. The completion of cleavage furrow ingression was considered to be time 0. The resulting intensity values were corrected for background by subtracting the average fluorescence intensity of 3 points of identical surface measured in areas devoid of cells, and then normalized to the initial value at time 0.

To determine the decrease of midbody Lifeact fluorescence intensity, we considered the first occurrence in which the signal dropped below 20% of the initial amount for at least two successive frames for each graph (i.e. for at least 5 min). We identified as a second actin spike an increase of the Lifeact intensity signal higher than 20%, after the initial drop and persisting for at least two consecutive frames.

ImageJ was used for quantitative analysis of protein localization (Rueden et al., 2017; Schindelin et al., 2012). For ANLN, F-actin and CHMP4B, an intensity profile was generated along the intercellular bridge; the ratio between fluorescence intensity at the secondary sites and the midbody was calculated; finally, a threshold was set in order to discriminate among positive and negative secondary ingression sites. Analyses requiring manual counting were performed on blinded samples. To determine F-actin intensity at the intercellular bridge (ICB), F-actin mean fluorescence intensity of a fixed area corresponding to the ICB was measured and normalized to the F-actin mean fluorescence intensity of the total cell. For analysis of F-actin localization in C3 transferase-treated synchronized cells, an intensity profile was created along the intercellular bridge and the distance between the lower intensity point of tubulin at the midbody and the lower intensity point of tubulin at the secondary ingression site (D1) was measured. We then measured the distance between the midbody and the

higher intensity point of F-actin (D2). We finally calculated the ratio between D2 and D1.

Statistics

Statistical analyses were performed using Microsoft Office Excel or GraphPad software. All the numbers represented by histograms were obtained by averaging all the data points contained in the replicates (with a comparable number of points per each replica). Unpaired Student's t-test and Chi-square were used to determine the P-value, as indicated.

Competing interests

The authors declare no competing or financial interests.

Author contributions

Conceptualization: A.D., G.E.B., F.T.B., A.M.C., G.P., F.D., M.G.; Methodology: A.D., F.M., M.G.; Validation: F.M.; Investigation: M.G.; Data curation: A.D., F.M., F.S., G.E.B., F.T.B., A.M.C., G.P., M.G.; Writing - original draft: M.G.; Writing - review & editing: A.D., F.M., G.E.B., F.T.B., A.M.C., G.P., F.D., M.G.; Visualization: M.G.; Supervision: F.D., M.G.; Project administration: F.D.; Funding acquisition: F.D.

Supplementary information

Supplementary information available online at
http://jcs.biologists.org/lookup/doi/10.1242/jcs.209080.supplemental

References

Agromayor, M. and Martin-Serrano, J. (2013). Knowing when to cut and run: mechanisms that control cytokinetic abscission. *Trends Cell Biol.* **23**, 433-441.

Bassi, Z. I., Verbrugghe, K. J., Capalbo, L., Gregory, S., Montembault, E., Glover, D. M. and D'Avino, P. P. (2011). Sticky/Citron kinase maintains proper RhoA localization at the cleavage site during cytokinesis. *J. Cell Biol.* **195**, 595-603.

Bassi, Z. I., Audusseau, M., Riparbelli, M. G., Callaini, G. and D'Avino, P. P. (2013). Citron kinase controls a molecular network required for midbody formation in cytokinesis. *Proc. Natl. Acad. Sci. USA* **110**, 9782-9787.

Dambournet, D., Machicoane, M., Chesneau, L., Sachse, M., Rocancourt, M., El Marjou, A., Formstecher, E., Salomon, R., Goud, B. and Echard, A. (2011). Rab35 GTPase and OCRL phosphatase remodel lipids and F-actin for successful cytokinesis. *Nat. Cell Biol.* **13**, 981-988.

Eggert, U. S., Mitchison, T. J. and Field, C. M. (2006). Animal cytokinesis: from parts list to mechanisms. *Annu. Rev. Biochem.* **75**, 543-566.

El Amine, N., Kechad, A., Jananji, S. and Hickson, G. R. X. (2013). Opposing actions of septins and Sticky on Anillin promote the transition from contractile to midbody ring. *J. Cell Biol.* **203**, 487-504.

Elia, N., Sougrat, R., Spurlin, T. A., Hurley, J. H. and Lippincott-Schwartz, J. (2011). Dynamics of endosomal sorting complex required for transport (ESCRT) machinery during cytokinesis and its role in abscission. *Proc. Natl. Acad. Sci. USA* **108**, 4846-4851.

Gai, M., Camera, P., Dema, A., Bianchi, F., Berto, G., Scarpa, E., Germena, G. and Di Cunto, F. (2011). Citron kinase controls abscission through RhoA and anillin. *Mol. Biol. Cell* **22**, 3768-3778.

Gruneberg, U., Neef, R., Li, X., Chan, E. H. Y., Chalamalasetty, R. B., Nigg, E. A. and Barr, F. A. (2006). KIF14 and citron kinase act together to promote efficient cytokinesis. *J. Cell Biol.* **172**, 363-372.

Guizetti, J., Schermelleh, L., Mäntler, J., Maar, S., Poser, I., Leonhardt, H., Müller-Reichert, T., Gerlich, D. W., Barr, F. A., Gruneberg, U. et al. (2011). Cortical constriction during abscission involves helices of ESCRT-III-dependent filaments. *Science* **331**, 1616-1620.

Hu, C.-K., Coughlin, M., Mitchison, T. J. and Doxsey, S. (2012). Midbody assembly and its regulation during cytokinesis. *Mol. Biol. Cell* **23**, 1024-1034.

McKenzie, C., Bassi, Z. I., Debski, J., Gottardo, M., Callaini, G., Dadlez, M. M. and D'Avino, P. P. (2016). Cross-regulation between Aurora B and Citron kinase controls midbody architecture in cytokinesis. *Open Biol.* **6**, 160019.

Mierzwa, B. and Gerlich, D. W. (2014). Cytokinetic abscission: molecular mechanisms and temporal control. *Dev. Cell* **31**, 525-538.

Piekny, A. J. and Glotzer, M. (2008). Anillin is a scaffold protein that links RhoA, actin, and myosin during cytokinesis. *Curr. Biol.* **18**, 30-36.

Pollard, T. D. (2010). Mechanics of cytokinesis in eukaryotes. *Curr. Opin. Cell Biol.* **22**, 50-56.

Renshaw, M. J., Liu, J., Lavoie, B. D. and Wilde, A. (2014). Anillin-dependent organization of septin filaments promotes intercellular bridge elongation and Chmp4B targeting to the abscission site. *Open Biol.* **4**, 130190.

Riedl, J., Crevenna, A. H., Kessenbrock, K., Yu, J. H., Neukirchen, D., Bista, M., Bradke, F., Jenne, D., Holak, T. A., Werb, Z. et al. (2008). Lifeact: a versatile marker to visualize F-actin. *Nat. Methods* **5**, 605-607.

Rueden, C. T., Schindelin, J., Hiner, M. C., DeZonia, B. E., Walter, A. E., Arena, E. T. and Eliceiri, K. W. (2017). ImageJ2: ImageJ for the next generation of scientific image data. *BMC Bioinformatics* **18**, 529.

Saurin, A. T., Durgan, J., Cameron, A. J., Faisal, A., Marber, M. S. and Parker, P. J. (2008). The regulated assembly of a PKCepsilon complex controls the completion of cytokinesis. *Nat. Cell Biol.* **10**, 891-901.

Schiel, J. A., Park, K., Morphew, M. K., Reid, E., Hoenger, A. and Prekeris, R. (2011). Endocytic membrane fusion and buckling-induced microtubule severing mediate cell abscission. *J. Cell Sci.* **124**, 1769-1769.

Schiel, J. A., Simon, G. C., Zaharris, C., Weisz, J., Castle, D., Wu, C. C. and Prekeris, R. (2012). FIP3-endosome-dependent formation of the secondary ingression mediates ESCRT-III recruitment during cytokinesis. *Nat. Cell Biol.* **14**, 1068-1078.

Schindelin, J., Arganda-Carreras, I., Frise, E., Kaynig, V., Longair, M., Pietzsch, T., Preibisch, S., Rueden, C., Saalfeld, S., Schmid, B. et al. (2012). Fiji: an open-source platform for biological-image analysis. *Nat. Methods* **9**, 676-682.

Sgrò, F., Bianchi, F. T., Falcone, M., Pallavicini, G., Gai, M., Chiotto, A. M. A., Berto, G. E., Turco, E., Chang, Y. J., Huttner, W. B. et al. (2016). Tissue-specific control of midbody microtubule stability by Citron kinase through modulation of TUBB3 phosphorylation. *Cell Death Differ.* **23**.

Watanabe, S., De Zan, T., Ishizaki, T. and Narumiya, S. (2013). Citron kinase mediates transition from constriction to abscission through its coiled-coil domain. *J. Cell Sci.* **126**, 1773-1784.